Hindawi
Shock and Vibration
Volume 2021, Article ID 9971761, 9 pages
https://doi.org/10.1155/2021/9971761

Research Article

The Comparative Study on the Damage Zones of Cylindrical and Spherical Charges in Rock and Soil

Qian Xu and Zhong-Qi Wang

State Key Laboratory of Explosion Science and Technology, Beijing Institute of Technology, Beijing 100081, China

Correspondence should be addressed to Qian Xu; chinaxuqian@126.com

Received 26 March 2021; Accepted 25 April 2021; Published 11 May 2021

Academic Editor: Feng Du

To compare the damage zones of spherical and cylindrical charges in rock and soil, a quasistatic spherical model was established to predict the characteristic dimension of the cavity. The results indicated that the damage zones of cylindrical charges were larger than those of spherical charges. Furthermore, the cavity development of two charges with different shapes was obtained by numerical simulation, and a comparison of the prediction results between the quasistatic model and numerical simulation was made. The comparison showed that the model could predict the damage zones exactly and faster than numerical simulation. Ultimately, the influence of explosions and soil media was discussed by the quasistatic model. It was observed that larger damage zones were generated by smaller values of the product of pressure and exponential expansion. However, the influence of soil media was complex, and larger damage zones were usually generated by the harder soil media.

1. Introduction

The problem of the damage zones caused by an explosion in the rock and soil has been widely investigated. The size of the damage zones affects the seismic wave field generated by the explosion; thus, the damage zones with different sizes are encountered in different engineering fields. In practical engineering, spherical charge and cylindrical charge are two commonly used charge forms; therefore, it is necessary to conduct a comparative study on the damage zones to provide a basis for the choice between these two charge forms.

The research methods for the damage zones caused by these two kinds of charge mainly include the analytical method, numerical analysis, and explosive test method in soil. Henrych, respectively, proposed the cavity analytical expressions for the rock and soil under quasiempirical, quasistatic, and dynamic conditions [1–6]. Zhang derived the analytical expressions for the crushed zone generated by two charge forms based on the theory of explosion shock wave and suggested that the size of the crushed zone was related to the initial charge radius [7]. Holmberg and Persson [8], Ouchterlony [9], Kanchibolta et al. [10], and Ouchterlony et al. [11] predicted the size of the broken area by a semiempirical formula that is broadly used in engineering fields. However, this formula is utilized for quantitative analysis with poor accuracy and cannot distinguish the types of geotechnical media. Forrestal and Tzou [12] and Voitenko [13] used explosion dynamics theory to calculate the damage area and, as a result, they obtained higher accuracy results. However, this calculation method was complicated and inefficient. Furthermore, the range of the generated plastic zone, which directly affects the characteristics of the seismic wave field, is not considered in the above methods. Moreover, the dynamic method often takes much more time in the process of calculating the damage zones, which is not suitable for the analysis of seismic wave field, while the quasistatic method can quickly calculate the damage zones and it is more suitable for the analysis of seismic wave field. Lin and Bai [14] studied the impact process of explosives in rock and soil and obtained the impact pressure and evolution process of the inner surface of the cavity during the expansion of the explosive cavity under the condition of spherical

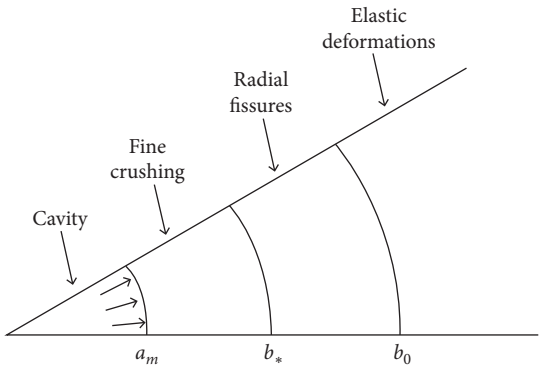

Figure 1: Distribution of different damage zones.

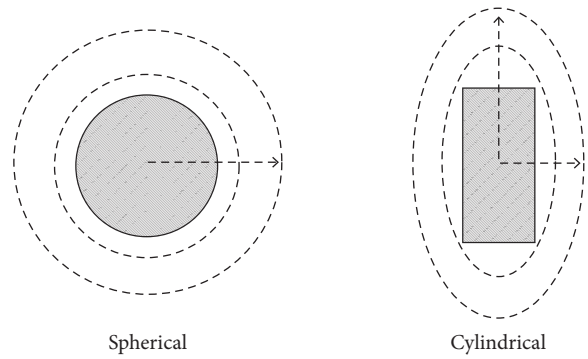

Figure 2: Explosive wave characteristics produced by two charge forms.

charge. This study provided a theoretical basis for the study of the internal surface pressure of cavity sources. Bergeron et al. [15] carried out a large number of experiments regarding the explosion in soil and made tangible progress. Luccioni [16] conducted a series of tests on explosives in the soil surface and near-surface. The study analyzed the influence of soil properties on the size of the explosion funnel. Fiserova [17] used the AUTODYN program to numerically simulate the dynamic response of explosives and compared the results with the analytical model given by Henrych. Luccioni and Ambrosini [18] and Ambrosini and Luccioni [19] utilized the AUTODYN program to perform numerical simulations regarding explosives in the ground and shallow burial conditions. Overall, the results of the development of the explosive cavity obtained from the numerical simulations are consistent with the experimental results.

Based on the quasistatic theory, this study established a prediction model for the damage zones of the spherical drug package, which was compared with the column-symmetric model established by Drukovanyi et al. [20]. The feasibility of the model was verified by comparing it with the numerical simulation method, and the effects of explosive properties and geotechnical medium on the damage zones were analyzed as well.

2. Prediction of Damage Zones

The process of explosives from blasting to finally forming elastic waves in the distance is accompanied by a series of chemical and physical changes. The energy keeps attenuating during the transmission process due to various dissipation mechanisms, showing the evolution from the powerful blast waves to elastic waves finally. This process is composed of four stages, which are hydrodynamic stage, geomaterial crushing stage, dynamic expansion stage, and elastic wave propagation stage. Meanwhile, the medium would have irreversible deformation under the strong explosion effects during the attenuation process, so that the geomaterial near the explosive source shows certain fluid properties under the impacts of huge energy. At the moment of explosion, a wave front could be pushed out from inside the explosion cave, which is in a shape the same as the explosive. With the development of the blast wave, its peak stress attenuates rapidly during the outward propagation process until below the ultimate failure strength of the geomaterial. At this moment, the geomaterial turns from the fluid stress state to the elastic-plastic stress state. And the attenuation of the stress wave continues until its peak value falls below a certain value, and the geomaterial transforms from the plastic state to the elastic state. In this case, the explosive source forms the explosion cavity area, plastic area, and an elastic area in sequence when it blasts in geomaterial along the energy transformation direction (Figure 1).

Since the explosion wave generated by the spherical charge explosion is a spherical wave and the cylindrical charge explosion produces a cylindrical explosion wave, therefore, under the same charge quantity, the two charge forms will produce different damage zones (Figure 2). To further investigate the effect of charge form on seismic wave field, it is necessary to compare the damage zones caused by spherical and cylindrical charges.

To predict the size of damage zones of different charge structures, a quasistatic model for damage zones prediction was established. In the model, there are several assumptions as follows: (1) The rock and soil medium are incompressible. (2) The change in the density of rock and soil caused by the explosion is ignored. (3) The formation of the explosive cavity and damage zones is instantaneous. (4) The detonation of explosives is instantaneous. As shown in Figure 1, a_m is the cavity radius, b_* is the radius of the crushed zone, and b_0 is the radius of the fracture zone. The whole region can be divided into three parts:

(1) Elastic zone: $b_0(t) \le r \le \infty$

(2) Cracked zone: $b_*(t) \le r \le b_0(t)$

(3) Crushed zone (cavity): $a_m(t) \le r \le b_*(t)$

2.1. Elastic Zone

2.1.1. Spherical Charge. Based on the above assumptions, the shear stress is zero and the annular stress is equal under the condition of spherical cavity expansion in the elastic medium; thus, the equilibrium equation can be expressed as follows:

$$\frac{\mathrm{d}\sigma_r}{\mathrm{d}r} + \frac{2\left(\sigma_r - \sigma_\phi\right)}{r} = 0, \tag{1}$$

where σ_γ is the radial stress, σ_φ is the annular stress, and r is the explosion center. Then, the strain (QUOTEε) can be expressed as $\varepsilon_r = \mathrm{d}u/\mathrm{d}r$ and $\varepsilon_\varphi = u/r$, where u is the radial displacement. Hooke's law is applied to elastic deformation area and its general form can be expressed as follows:

$$\sigma_{ij} = 2\mu\varepsilon_{ij} + \lambda\theta\delta_{ij}. \tag{2}$$

μ and λ are Lame's coefficients, and the stress in the equilibrium equation is expressed as a function of displacement as follows:

$$\frac{\lambda}{2\mu} + \frac{\mathrm{d}\theta}{\mathrm{d}r} + \frac{\mathrm{d}}{\mathrm{d}r}\left[\frac{\mathrm{d}u}{\mathrm{d}r} + \frac{3u}{r}\right] = 0, \tag{3}$$

where θ is the volumetric strain, and the volumetric strain in the previous part of the formula is 0. In the inner boundary of the elastic area, the shear stress is limited by the tensile strength (σ_0) of the rock mass and the radial displacement becomes

$$u = \frac{1}{2\mu}\sigma_0 b_0\left(\frac{b_0}{r}\right)^2. \tag{4}$$

Therefore, in the elastic region, the displacement u_0 on the boundary b_0 can be expressed as follows:

$$u_0(t) = \frac{1}{2\mu}\sigma_0 b_0(t). \tag{5}$$

2.1.2. Cylindrical Charge. According to the above assumptions, the equilibrium equation under the condition of cylindrical charge can be expressed as follows:

$$\frac{\mathrm{d}\sigma_r}{\mathrm{d}r} + \frac{\left(\sigma_r - \sigma_\phi\right)}{r} = 0. \tag{6}$$

The displacement u_0 on the boundary of the elastic region b_0 can be expressed as follows:

$$u_0(t) = \frac{1}{2\mu}\sigma_0 b_0(t). \tag{7}$$

2.2. Fracture Zone

2.2.1. Spherical Charge. The annular stress is zero in the radial fracture zone; thus, the equilibrium equation is presented as follows:

$$\frac{\mathrm{d}\sigma_r}{\mathrm{d}r} + \frac{2\sigma_r}{r} = 0. \tag{8}$$

At the boundary of region 3, $\sigma_r(b0) = -\sigma_0$, and at the boundary of region 1, $\sigma_r(b^*) = -\sigma^*$, where σ^* is the compressive strength. By integrating the above equation, we can obtain the following equation:

$$\sigma_0 b_0^2 = \sigma_* b_*^2. \tag{9}$$

Then, the boundary at region 2 is expressed as follows:

$$u_*(t) = u_0(t) + \int_{b_0}^{b_*} \varepsilon_r \mathrm{d}r. \tag{10}$$

From the stress-strain relationship of $\sigma_r = 2\mu\varepsilon$, the particle vibration velocity u is expressed as follows:

$$u_*(t) = \frac{1}{2\mu}\sigma_* b_*. \tag{11}$$

2.2.2. Cylindrical Charge. Similarly, the simplified equilibrium equation of cylindrical charge is expressed as follows:

$$\frac{\mathrm{d}\sigma_r}{\mathrm{d}r} + \frac{\sigma_r - \sigma_\phi}{r} = 0. \tag{12}$$

At the boundary of region 3, $\sigma_r(b_0) = -\sigma_0$, and at the boundary of region 1, $\sigma_r(b^*) = -\sigma^*$, where σ^* is the compressive strength. By integrating the above equation, we have

$$\sigma_0 b_0 = \sigma_* b_*. \tag{13}$$

From the stress-strain relationship of $\sigma_\mathrm{r} = 2\mu\varepsilon$, the particle vibration velocity u is expressed as follows:

$$u_*(t) = \frac{1}{2\mu}\sigma_* b_*\left[1 + \mathrm{In}\left(\frac{\sigma_*}{\sigma_0}\right)\right]. \tag{14}$$

2.3. Crushed Zone. In the crushed zone, the rock and soil are in close contact with the explosive, and the instantaneous pressure generated by the explosion is far greater than the compressive strength of rock and soil. Therefore, in this region, significant plastic deformation, fracture, and other phenomena will appear on the medium. At present, the prediction of this area is very different, and it is generally believed that the radius of this area is about 3 to 5 times the charge radius. To describe the destruction of rock and soil in the crushed zone, a granular incompressible medium model with cohesive force is used. The simplified Mohr–Coulomb failure criterion is as follows:

$$\left|\tau_{\max}\right| = -f\sigma + k, \tag{15}$$

where $\tau_{\max}$ is shear strength, f is the internal friction coefficient, and k is cohesion. The shear stress at the time of the destruction is the maximum shear stress and the normal stress is $\sigma = (\sigma_\varphi + \sigma_r)/2$. Considering the incompressible optimal condition, the relationship is as follows: $\sigma_z = (\sigma_\varphi + \sigma_r)/2$. By substituting this equation into equation (9), we have

$$\sigma_\varphi = \alpha\sigma_r + \beta, \tag{16}$$

where $\alpha = (1 - f)/(1 + f)$, $\beta = 2k/(1 + f)$.

2.3.1. Spherical Charge. By substituting equation (16) into the spherical equilibrium equation and considering the boundary conditions, $r = b_*$, $\sigma_r = -\sigma_*$, we have

$$\sigma_r = \frac{\beta}{1-\alpha} - \left[\sigma_* + \frac{\beta}{1-\alpha}\right]\left(\frac{b_*}{r}\right)^{2(1-\alpha)}. \tag{17}$$

The pressure on the wall of the chamber is expressed as follows:

$$P = -\frac{k}{f} + \left[\sigma_* + \frac{k}{f}\right]\left(\frac{b_*}{a}\right)^{(4f/(1+f))}. \tag{18}$$

After applying the incompressible conditions and calculating the boundary $r = b_*$, we have

$$u_*(t) = \frac{1}{4\mu}\sigma_* b_* \left[3 - \frac{\sigma_*}{\sigma_0}\right]. \tag{19}$$

Because $\partial u/\partial r \ll 1$, the velocity on the wall of the chamber can be obtained by establishing the momentum equation:

$$v(a) = \frac{\mathrm{d}a}{\mathrm{d}t}. \tag{20}$$

When $t = 0$, the rupture at the boundary of the chamber begins to occur, then $a = b_* = a_*$, and we can obtain the following equation:

$$b_*^3 = L\left(\frac{a^3}{3} - a_*^3\left[\frac{1}{3} - \frac{1}{L}\right]\right). \tag{21}$$

Then, $L = 2\mu/\sigma_*$, and because $a \gg a_*$, we have

$$\frac{b_*}{a} = \sqrt[3]{\frac{2\mu}{3\sigma_*}} = \sqrt[3]{\frac{L}{3}\sqrt{b^2 - 4ac}}. \tag{22}$$

Thus, the detonation pressure P_m in the largest detonation chamber is expressed as follows:

$$P_m = -\frac{k}{f} + \left[\sigma_* + \frac{k}{f}\right]\left(\frac{L}{3}\right)^{(4f/(3(1+f)))}. \tag{23}$$

According to the adiabatic law, the pressure relationship on the blasting chamber is $P_m(a_m)^{3\gamma} = P_0(a_0)^{3\gamma}$, where a_0 is the charge radius, P_0 is the instantaneous pressure of the initial explosion, and γ is the explosive expansion index. The maximum radius of the blasting chamber is computed by the following equation:

$$a_m = a_0\left(\frac{P_0}{P_m}\right)^{(1/3\gamma)}. \tag{24}$$

We can obtain the size of the maximum crushed zone b_* as follows:

$$b_* = a_0\left(\frac{P_0}{-(k/f) + [\sigma_* + (k/f)]L^{(4f/(3(1+f)))}}\right)^{(1/3\gamma)}\sqrt[3]{\frac{2\mu}{3\sigma_*}}. \tag{25}$$

The range of radial fracture zone b_0 is expressed as follows:

$$b_0 = \left(\frac{\sigma_*}{\sigma_0}\right)^{(1/2)} b_*. \tag{26}$$

Introduce the linear radial strain and hoop strain according to the spherical symmetry and linear theory to simplify the motion equation as follows:

$$\frac{\partial^2 u}{\partial r^2} + \frac{2}{r}\frac{\partial u}{\partial r} - 2\frac{u}{r^2} = \frac{1}{c^2}\frac{\partial^2 u}{\partial t^2}. \tag{27}$$

The solution of this equation can describe the forced vibration of the particle under viscous damping, and its general form is

$$U(r,t) = e^{-(\eta^2\tau)/\rho_{\mathrm{soil}}cb_*}\left[\left(\frac{P_0 b_*^2 c}{\eta\kappa r^2} - \frac{\eta P_0 b_*}{\kappa\rho_{\mathrm{soil}}cr}\right)\sin\frac{\eta\kappa\tau}{\rho_{\mathrm{soil}}cb_0} + \frac{P_0 b_*}{\rho_{\mathrm{soil}}cb_0}\cos\frac{\eta\kappa\tau}{\rho_{\mathrm{soil}}cb_0}\right], \tag{28}$$

where

$$\eta^2 = \frac{2(1-2\sigma)\rho_{\mathrm{soil}}c^2 + 3(1-\sigma)\gamma P_0}{2(1-\sigma)},$$

$$\kappa^2 = \frac{2\rho_{\mathrm{soil}}c^2 - 3(1-\sigma)\gamma P_0}{2(1-\sigma)}, \tag{29}$$

$$\tau = t - \frac{r - b_0}{c}.$$

2.3.2. Cylindrical Charge. By substituting equation (16) into the spherical equilibrium equation and considering the boundary conditions, $r = b_*$, $\sigma_r = -\sigma_*$, we have

$$\sigma_r = \frac{k}{f} - \left[\sigma_* + \frac{k}{f}\right]\left(\frac{b_*}{r}\right)^{(2f/(1+f))}. \tag{30}$$

The pressure on the wall of the chamber is expressed as follows:

$$P = \frac{k}{f} + \left[\sigma_* + \frac{k}{f}\right]\left(\frac{b_*}{r}\right)^{(2f/(1+f))}. \tag{31}$$

By applying the incompressible conditions, we have

$$u_*(t) = \frac{1}{2\mu}\sigma_* b_* \left[1 + \mathrm{In}\left(\frac{\sigma_*}{\sigma_0}\right)\right]. \tag{32}$$

Now, let us consider:

Table 1: Characteristic parameters of TNT.

Classification of explosive	Explosive velocity (σ_*)	Density (σ_*)	Initial pressure (GPa)	Expansion index
TNT	6900	1650	9.82	3.15

Table 2: Characteristic parameters of sandy clay.

Categories of medium	σ_* (MPa)	σ_0 (MPa)	μ (GPa)	f	k (kPa)	ρ (kg/m3)
Sandy clay	11.6	2	0.16	0.2	50	1600

Table 3: Contrast of damage zones between spherical and cylindrical charges.

Type of charge	Radius of charge (m)	Radius of cavity (m)	Crushing zone (m)	Fracture zone (m)
Cylindrical	0.0580	0. 155	0.361	2.093
Spherical	0.0527	0.141	0.295	1.713

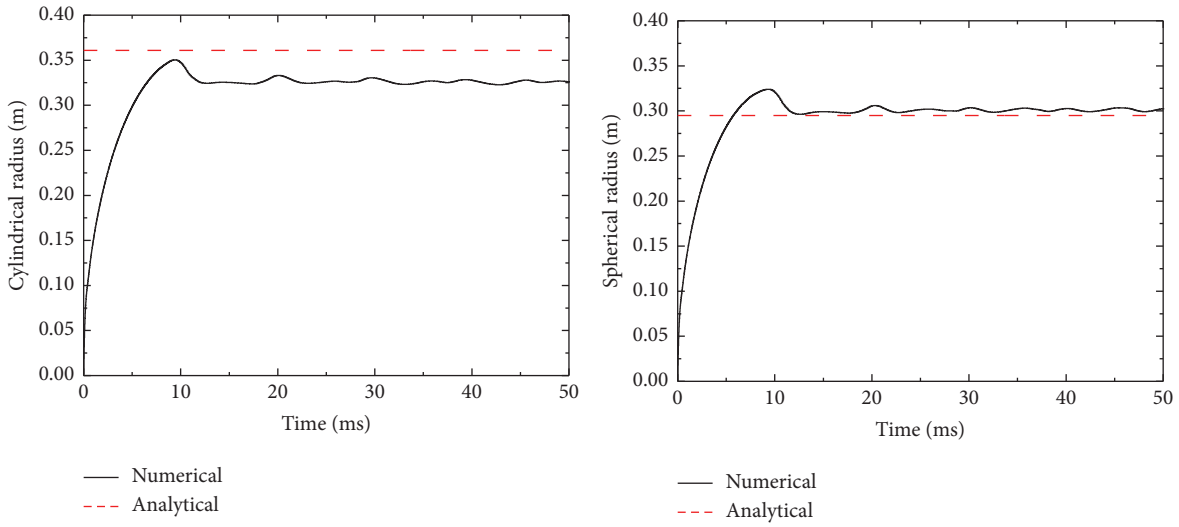

Figure 3: Scope of damage zones of cylindrical and spherical charges.

$$\frac{b_*}{a} = \sqrt{\frac{\mu}{\sigma_*\left[1 + \mathrm{In}\sigma_*/\sigma_0\right]}} = \sqrt{L}. \tag{33}$$

Therefore, the detonation pressure P_m in the largest detonation chamber is

$$P_m = -\frac{k}{f} + \left[\sigma_* + \frac{k}{f}\right] L^{2f/(1+f)}. \tag{34}$$

According to the adiabatic law, the pressure relationship on the blasting chamber is $P_m (a_m)^{3\gamma} = P_0 (a_0)^{3\gamma}$, where a_0 is the charge radius, P_0 is the instantaneous pressure of the initial explosion, and γ is the explosive expansion index. The maximum radius of the blasting chamber is calculated by the following equation:

$$a_{mc} = a_0 \left(\frac{P_0}{P_m}\right)^{(1/2\gamma)}. \tag{35}$$

We can obtain the size of the maximum crushed zone b_* as follows:

$$b_{*m} = a_0 \left(\frac{P_0}{-(k/f) + \left[\sigma_* + (k/f)\right] L^{2f/(1+f)}}\right)^{1/2\gamma} \sqrt{\frac{\mu}{\sigma_*\left[1 + \ln\left(\sigma_*/\sigma_0\right)\right]}}. \tag{36}$$

The range of radial fracture zone b_0 is expressed as follows:

$$b_{0m} = \left(\frac{\sigma_*}{\sigma_0}\right) b_{*m}. \tag{37}$$

3. Contrastive Analysis of Damage Zones

3.1. Example Analysis. According to the calculation model of damage zones under two charge forms obtained in this study, TNT explosion in ordinary sandy clay under two charge forms was calculated, among which the characteristic parameters of TNT and siltstone are shown in Tables 1 and 2, and the calculation results are shown in Table 3.

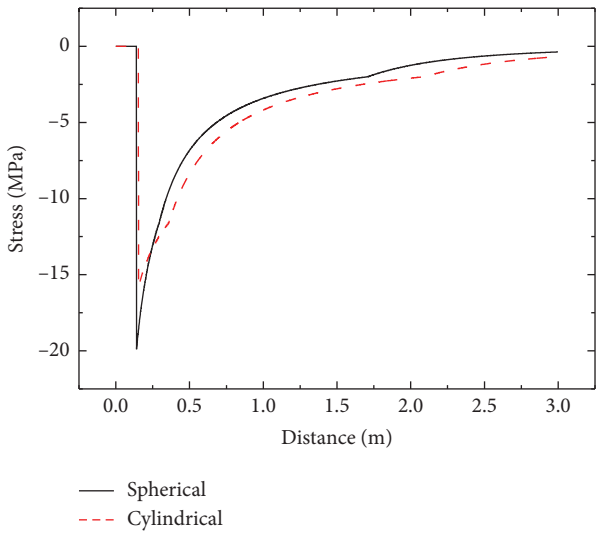

Figure 4: Stress distribution of different charge structures in the medium.

Table 4: Characteristic parameters of different explosives.

Classification of explosive	Explosive velocity (σ_*)	Density (σ_*)	Pressure (GPa)	Expansion index
RDX	8300	1700	14.64	3.4
TNT	6900	1650	9.82	3.15
TL	4500	1500	3.80	2.6
BP	3100	1500	1.81	1.8

It can be seen from the calculated results that when the charge amount was the same, the size of the destructed zone produced by the two charge structures in the radial direction was different, and the radius of the destructed zone produced by the spherical charge was smaller than that of the cylindrical charge. This was because of the obvious directivity of the cylindrical charge when it exploded. Hence, the strong pressure was generated in the radial direction, and thus, the damage zones generated in the radial direction were greater than those caused by the spherical charge.

To further compare the size of the damage zones caused by the two charge forms, the software AUTODYN was employed to simulate the explosion process of spherical and cylindrical charges in the solid medium. The initial dosage of the two charge forms was 1 kg. The linear material model and von Mises intensity model were selected for the geotechnical medium. The model parameters were obtained through literature. The JWL equation of state that exists in the AUTODYN software was utilized to describe the explosives. The comparison between the calculated results and the predicted results of the quasistatic model is shown in Figure 3.

The results of the radius of damage zones obtained by the quasistatic analytical method were similar to the numerical simulation method (Figure 3). The cavity generated by the cylindrical charge was estimated to be 0.326 m by numerical simulation and 0.361 m by the analytical model. The cavity generated by spherical charge was estimated to be 0.309 m by numerical simulation and 0.295 m by the analytical model. By comparing the two methods, it was observed that the analytical model could predict the radius of the damage

Table 5: Calculation results of different explosives.

Categories of explosives	Cylindrical charge		Spherical charge	
	b_*/a_0	b/a_0	b_*/a_0	b/a_0
RDX	6.13	35.57	5.53	23.32
TNT	6.24	36.17	5.60	23.50
TL	6.45	37.43	5.75	23.85
BP	8.40	48.73	7.32	27.63

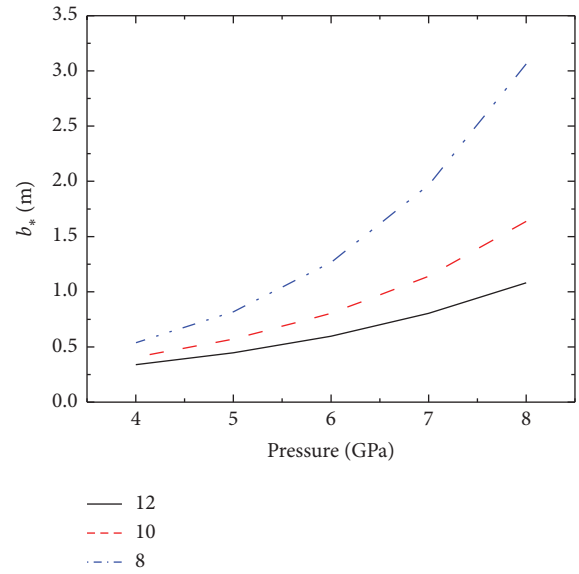

Figure 5: Change curve of the crushed zone under different $P^*\gamma$ values of the cylindrical charge.

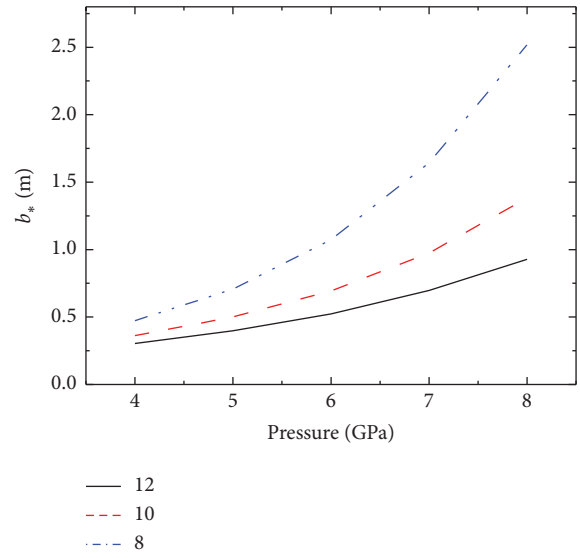

Figure 6: Change curve of the crushed zone under different $P^*\gamma$ values of the spherical charge.

Table 6: Characteristic parameters of different rock and soil types.

Categories of medium	σ_* (kg/cm^2)	σ_0 (kg/cm^2)	μ (GPa)	f	k (kg/cm^2)	ρ (kg/m^3)
Siltstone	2000	143	1.13	0.267	800	2600
Diabase	3090	560	5.76	0.67	1000	2800
Concrete	950	160	1.49	0.44	395	2070
Limestone	620	63	2.10	0.42	420	1900

Table 7: Scope of damage zones of two charge forms under different medium conditions.

Categories of medium	Cylindrical charge		Spherical charge	
	b_*/a_0	b/a_0	b_*/a_0	b/a_0
Siltstone	5.22	72.9	2.51	9.37
Diabase	9.15	50.56	3.02	6.99
Concrete	10.36	59.7	3.57	8.7
Limestone	14.0	137.6	4.50	14.12

zones quickly and easily. Moreover, the conclusion that the cavity radius of spherical charge in the radial direction was smaller than that of cylindrical charge could also be verified. To further understand the radial destruction caused by different charge structures, it was necessary to analyze the stress distribution in the medium. The analytical model was used to calculate the stress distribution generated by the two charges in the medium. The results are shown in Figure 4.

Figure 4 shows that the stress peak on the medium was larger because of the smaller damage zones caused by the spherical charge and the less energy consumed by the destructed rock and soil. It was found from the calculation that the stress peak generated by the cylindrical charge on the cavity surface was about 75% that of the spherical charge. However, with the propagation of the explosion wave, because of the different energy release characteristics between the spherical and cylindrical waves, the stress attenuation of the spherical charge acting on the medium was faster than that of the cylindrical charge. Therefore, they had different effects on the characteristics of particle vibration.

3.2. Effect of Explosive Properties on Damage Zones. In engineering practice, the damage zones with different sizes are encountered in different engineering fields; thus, it is necessary to master the control method of the damage zones. According to the analysis of the analytical model, the scope of the damage zones was primarily affected by the properties of explosives and rock and soil. The detonation pressure and expansion index of explosives certainly affected the size of the damage zones. Table 4 shows the characteristic parameters of four common explosives.

Considering sandy clay as the rock and soil medium, the damage zones formed by four different explosives are shown in Table 5.

The initial pressure of the explosion increased with the detonation speed, but the calculation results from Table 5 indicated that the greater the detonation speed, the smaller the damage zones. This was because the scope of the damage zones was related not only to the initial pressure of the explosive but also to the expansion index of the explosive. Generally speaking, the greater the explosive detonation speed was, the smaller the expansion index was. Therefore, when analyzing the impact of explosive properties on the damage zones, the initial pressure and expansion index should be considered together. Figures 5 and 6, respectively, exhibit the influence of the product of different expansion indices and initial pressures on the size of the damage zones under cylindrical and spherical charge forms.

Figures 5 and 6 display that when the $P^*\gamma$ value decreased, the size of the blasting chamber under the two charge conditions was larger. Moreover, when the $P^*\gamma$ value remained unchanged, the size of the explosive chamber increased with the increase of the initial pressure of the explosive. Therefore, the initial explosion pressure and expansion index of the explosive can be changed in the process of controlling the damage zones.

3.3. Effects of Rock and Soil on the Damage Zones. The change of the properties of rock and soil would also affect the size of the damage zones. Table 6 shows the characteristic parameters of four different rocks and soils. The calculation of damage zones of two charge forms under the condition of TNT charge was performed, respectively. The results are shown in Table 7.

The calculation results in Table 7 suggest that the size of the blasting chamber gradually increased with the decrease of the strength of the rock and soil, but there was no certain linear rule between the two because of a large number of rock and soil parameters that affected the results. The larger the strength of the medium, the more energy was needed to expand the cavity, thus, the smaller the size of the cavity was. Under the same conditions, the size of the crushed zone and the fracture zone formed by the cylindrical charge was larger than that formed by the spherical charge.

4. Discussion

An explosive cavity test was carried out to test the accuracy of the quasistatic model in predicting the size of the explosion cavity. The experimental results are compared with the quasistatic results. 1 kg TNT and 2 kg TNT were exploded in silty clay; the explosion cavity of the experiment is shown in Figure 7. Measuring the cavity radius of vertical and horizontal, the results of cavity radius calculated by the quasistatic method and measured radius are shown in Table 8.

The calculation results in Table 8 suggest that the difference between the quasistatic model result and the

Figure 7: Explosive cavity in the soil.

Table 8: Result of the explosion cavity test.

Soil type	Explosive quality (Kg)	Explosive radius (cm)	Radius of explosive cavity (cm)		Radius of quasistatic method
			Vertical	Horizontal	
Silt clay	1	5.3	40.8	38.5	36.43
Silt clay	1	5.3	41.5	39.5	36.43
Silt clay	2	6.7	49.5	50.5	42.04
Silt clay	2	6.7	48.5	48.0	42.04

measured result is about 5.4%~12.0%. This shows that the quasistatic model has a small gap with the results of the cavity radius obtained by the other two methods. The main reason for the difference value is the accuracy of geotechnical parameters. To reduce the difference between the theoretical model results and the measured results, it is necessary to study the acquisition of near-surface geotechnical parameters.

5. Conclusion

(1) The quasistatic analytical method was used to predict the damage zones of spherical and cylindrical charges. The results showed that the radial damage zones of the spherical charge were smaller than those of the cylindrical charge under the same conditions. By comparing with the results of numerical simulation, it was proved that the analytical model can quickly and easily solve the damage zones caused by different drug packages.

(2) The analytical model was utilized to calculate the stress distribution of the two charges in the medium. Because the damage zones of the spherical charge were small, the stress peak in the medium was larger than that of the cylindrical charge.

(3) This model was employed to analyze the impact of explosives and rock and soil on the damage zones. We found that the smaller the expansion index of explosives, the greater the initial explosion pressure, and the larger the damage zones. Therefore, the influence of $P^*\gamma$ on the damage zones was comprehensively examined. The smaller the value was, the larger the damage zones were. Furthermore, the parameters of rock and soil had an impact on the damage zones. It was observed from the results that there were many parameters of rock and soil that had no regular law. By selecting the different media in siltstone, diabase, concrete, and limestone, we found that the smaller the medium's strength, the larger the damage zones.

(4) In different engineering fields, the size requirements of the damage zones are also different. For example, in the field of seismic exploration, it is necessary to control the scope of the plastic damage zones to obtain stronger seismic waves, while in the mine blasting, it is necessary to strengthen the rock-breaking ability of the charge package and to reduce the blasting seismic effect. According to their different requirements, the spherical charge is more suitable for seismic exploration and the cylindrical charge is more suitable for mine blasting.

Data Availability

The data are available and included within the article; the data supporting the conclusions of this study are also available from the corresponding author.

Conflicts of Interest

The authors declare no conflicts of interest.

Acknowledgments

The authors thank the State Key Laboratory of Explosion Science and Technology in Beijing Institute of Technology.

This work was supported by the National Natural Science Foundation of China (no. 51678050) and the National Key R&D Program of China (no. 2017YFC0804702).

References

[1] J. Henrych and G. R. Abrahamson, "The dynamics of explosion and its use," *Journal of Applied Mechanics*, vol. 47, no. 1, pp. 217-218, 1980.

[2] Y. Wang, W. K. Feng, R. L. Hu, and C. H. Li, "Fracture evolution and energy characteristics during marble failure under triaxial fatigue cyclic and confining pressure unloading (FC-CPU) conditions," *Rock Mechanics and Rock Engineering*, vol. 54, no. 2, pp. 799–818, 2021.

[3] B. Li, R. Bao, Y. Wang, R. Liu, and C. Zhao, "Permeability evolution of two-dimensional fracture networks during shear under constant normal stiffness boundary conditions," *Rock Mechanics and Rock Engineering*, vol. 54, no. 3, pp. 1–20, 2021.

[4] Q. Wang, H. Gao, B. Jiang, S. Li, M. He, and Q. Qin, "In-situ test and bolt-grouting design evaluation method of underground engineering based on digital drilling," *International Journal of Rock Mechanics and Mining Sciences*, vol. 138, Article ID 104575, 2021.

[5] Q. Wang, Q. Qin, B. Jiang et al., "Mechanized construction of fabricated arches for large-diameter tunnels," *Automation in Construction*, vol. 124, Article ID 103583, 2021.

[6] A. Li, F. Dai, Y. Liu, H. Du, and R. Jiang, "Dynamic stability evaluation of underground cavern sidewalls against flexural toppling considering excavation-induced damage," *Tunnelling and Underground Space Technology*, vol. 112, Article ID 103903, 2021.

[7] Q. Zhang, "The crushed area of rock blasting and its cavity expansion," *Explosion and Shock Waves*, vol. 10, no. 1, pp. 68–75, 1990.

[8] R. Holmberg and P. A. Persson, "The Swedish approach to contour blasting," in *Proceedings of IVth Conference on Explosives and Blasting Technique*, pp. 113–127, New Orleans, LA, USA, December 1978.

[9] F. Ouchterlony, "Prediction of crack lengths in rock after cautious blasting with zero inter-hole delay," *Fragblast*, vol. 1, no. 4, pp. 417–444, 1997.

[10] S. S. Kanchibotla, W. Valery, and S. Morrell, "Modeling fines in blast fragmentation and its impact on crushing and grinding," *AusIMM*, vol. 99, no. 5, pp. 137–144, 1999.

[11] F. Ouchterlony, M. Olsson, and I. Bergqvist, "Towards new Swedish recommendations for cautious perimeter blasting," *Fragblast*, vol. 6, no. 2, pp. 235–261, 2002.

[12] M. J. Forrestal and D. Y. Tzou, "A spherical cavity-expansion penetration model for concrete targets," *International Journal of Solids and Structures*, vol. 34, no. 31-32, pp. 4127–4146, 1997.

[13] Y. I. Voitenko, "Fracture of solids by weak blasts," *Combustion, Explosion, and Shock Waves*, vol. 31, no. 4, pp. 492–499, 1995.

[14] D. C. Lin and C. H. Bai, *Explosion Seismic Effect*, pp. 3-4, Geological Publishing Housepp, Haidian, China, 2007.

[15] D. Bergeron, R. Walker, and C. Coffey, *Detonation of 100-gram Anti-personnel Mine Surrogate Charges in Sand-A Test Case for Computer Code Validation*, pp. 2–20, Defence Research Reports, DRDO Bavan, New Delhi, 1998.

[16] B. Luccioni, "Craters produced by underground explosions," *Computers & Structures*, vol. 87, no. 21-22, pp. 1366–1373, 2009.

[17] D. Fiserova, *Numerical Analysis of Buried Mine Explosions with Emphasis on Effect on Soil Properties on Loading*, Cranfield University, Cranfield, UK, 2006.

[18] B. Luccioni and R. D. Ambrosini, "Effect of buried explosions," *Computational Mechanics*, vol. 26, pp. 2656–2673, 2007.

[19] R. D. Ambrosini and B. Luccioni, "Craters produced by large-scale explosions," *Computational Mechanics*, vol. 26, pp. 1801–1822, 2008.

[20] M. F. Drukovanyi, V. S. Kravtsov, Y. E. Chernyavskii, V. V. Shelenok, N. P. Reva, and S. N. Zver'kov, "Calculation of fracture zones created by exploding cylindrical charges in ledge rocks," *Soviet Mining Science*, vol. 12, no. 3, pp. 292–295, 1976.